Construction of Carbon-based Frustrated Lewis Pairs for Sustainable Hydrogen Evolution through Heteroatom Bond Formation

Lulu Bai [a,b], Yashi Chen [a,b*], Zhen Wang [a,b], Saijia Hao [a,b], Chenhong Xiao [a,b], Qingjun Chen [c], Lei Liu [a,b*]

a Center for Computational Chemistry, School of Chemistry and Chemical Engineering, Wuhan Textile University, Wuhan 430200, China

b Hubei Key Laboratory of Biomass Fibers and Eco-Dyeing & Finishing, College of Chemistry and Chemical Engineering, Wuhan Textile University, Wuhan, 430200 China.

c Key Laboratory of Rare Earths, Chinese Academy of Sciences, Ganjiang Innovation Academy, Chinese Academy of Sciences, Ganzhou 341000, China

** Corresponding authors:*

Lei Liu: liulei@wtu.edu.cn; liulei3039@gmail.com

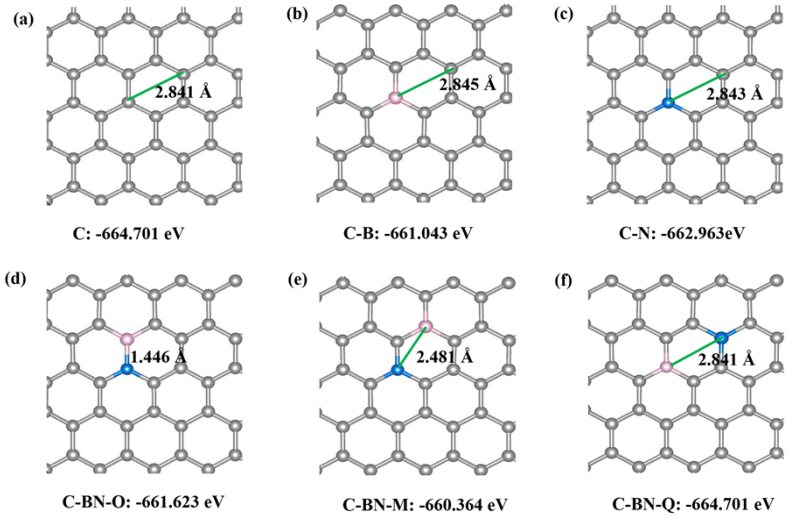

Fig. S1 (a) C, (b) BC, (c) NC, (d) BNC-ortho-positions, (e) BNC-meta-positions, and (f) BNC-para-positions after geometry optimization.

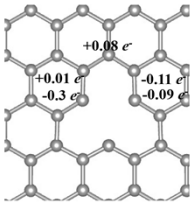

Fig. S2 Bader charges for the C-d carbon atom (gray). The values indicate electron gains or losses for each atom.

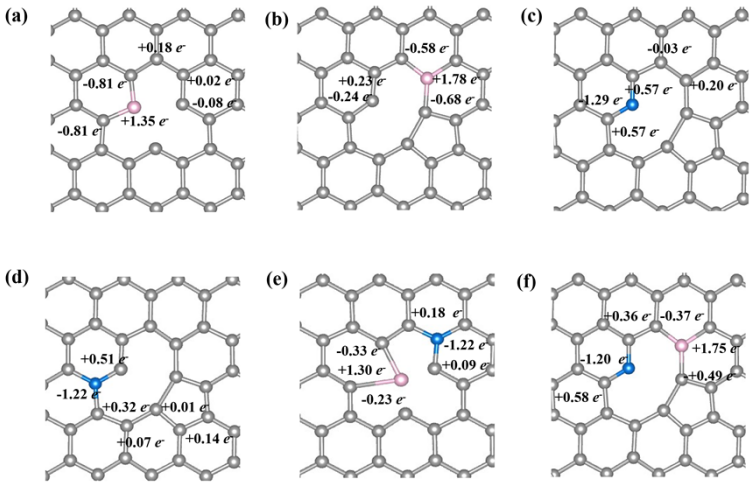

Fig. S3 Charge transfer effects between dopants. Bader charge of (a) B_{sp2}-d, (b) B_{sp3}-d, (c) N_{sp2}-d, (d) N_{sp3}-d, (e) $B_{sp2}N_{sp3}$-d, and (f) $B_{sp3}N_{sp2}$-d configurations. Positive and negative values represent electron loss and gain, respectively

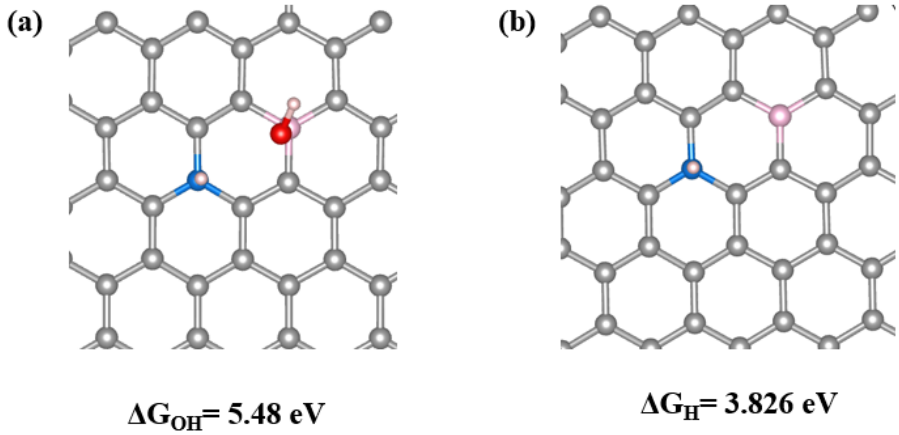

Fig. S4 (a) Reaction free energy of the hydrolysis pathway of FLPs on the *para*-positioned B/N atomic pairs with no defects. (b) HER free energy diagram of the *para*-positioned B/N atomic pairs with no defects.

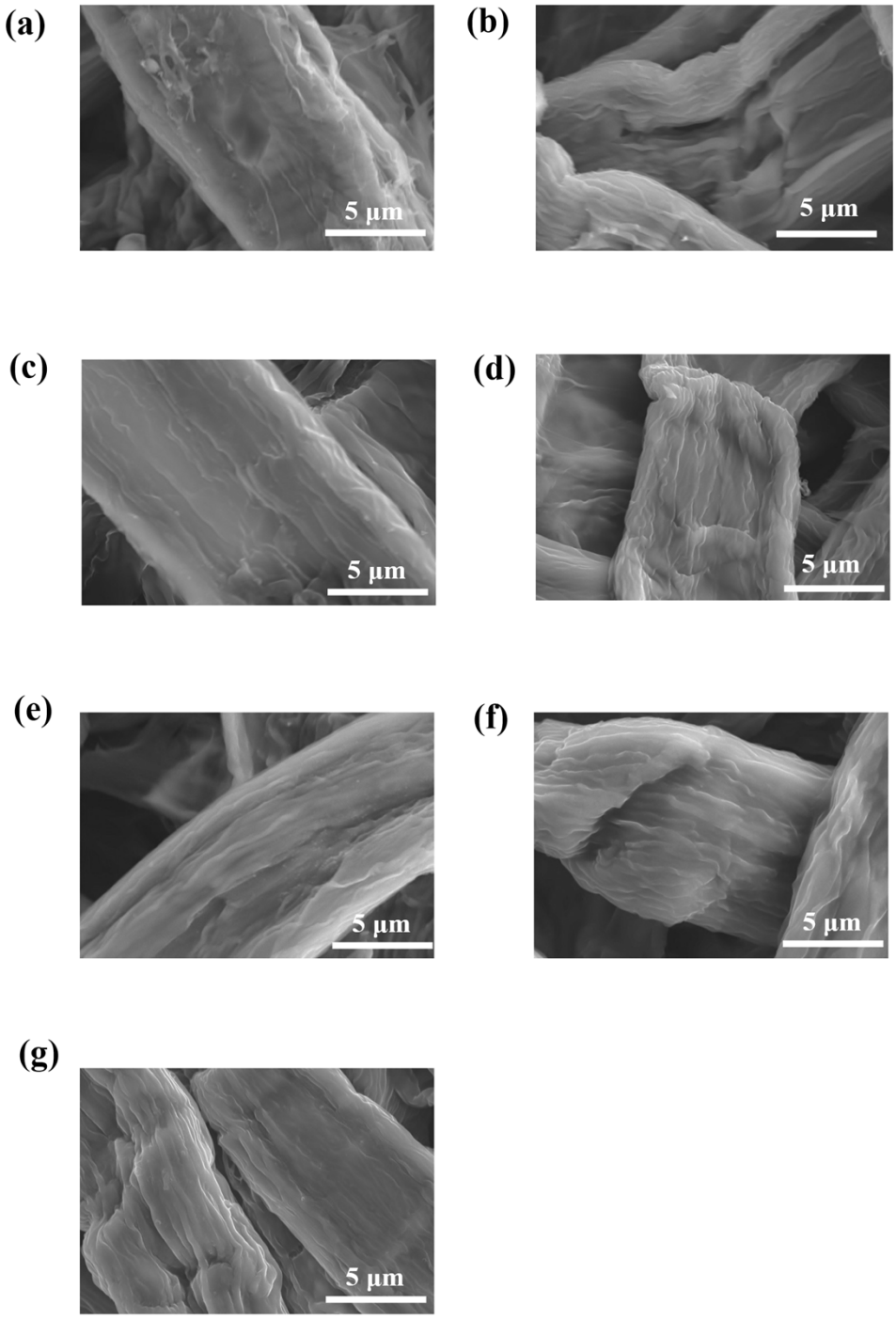

Fig. S5 SEM images of (a) C_{800}, (b) B_1C_{800}, (c) N_3C_{800}, (d) $B_1N_2C_{800}$, (e) $B_1N_4C_{800}$ (f) $B_1N_3C_{900}$, and (g) $B_1N_3C_{700}$.

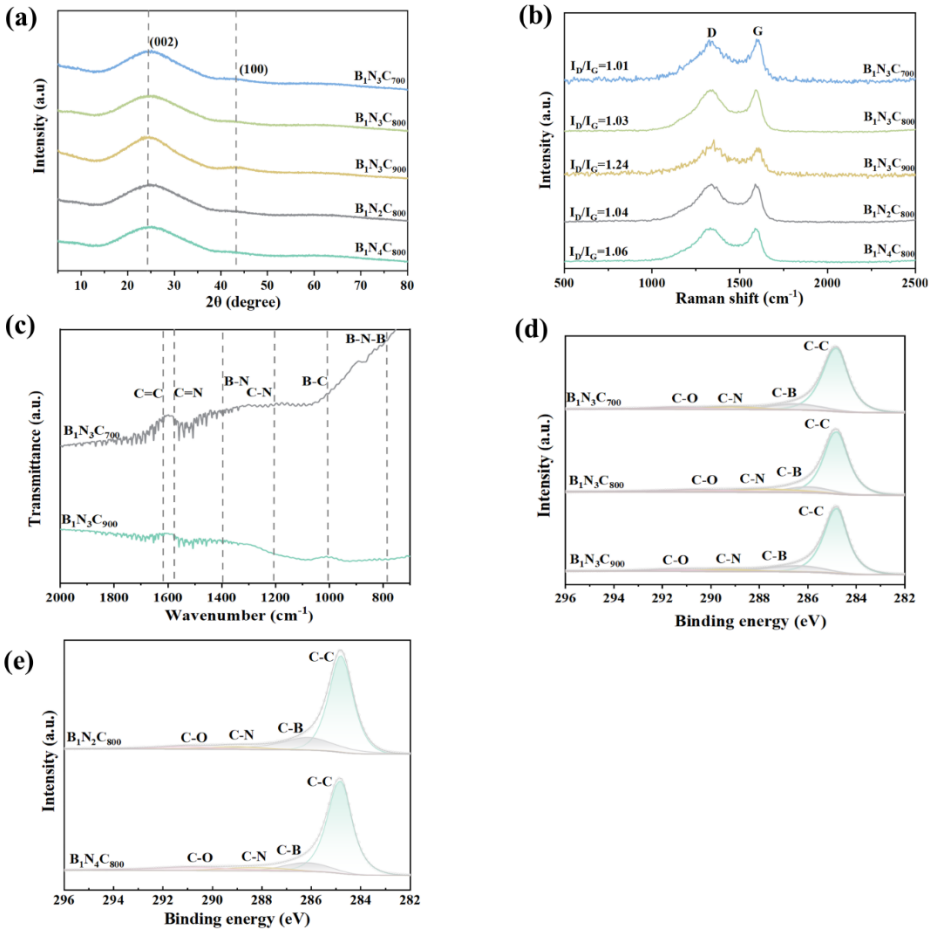

Fig. S6 (a) XRD patterns of $B_1N_3C_{700}$, $B_1N_3C_{800}$, $B_1N_3C_{900}$, $B_1N_2C_{800}$, and $B_1N_4C_{800}$. The Raman (b) and FT-IR spectra (c) of $B_1N_3C_{700}$, $B_1N_3C_{800}$, $B_1N_3C_{900}$, $B_1N_2C_{800}$, and $B_1N_4C_{800}$. (d) High resolution C 1s XPS spectra for $B_1N_3C_{700}$, $B_1N_3C_{800}$, $B_1N_3C_{900}$, (e) $B_1N_2C_{800}$, and $B_1N_4C_{800}$.

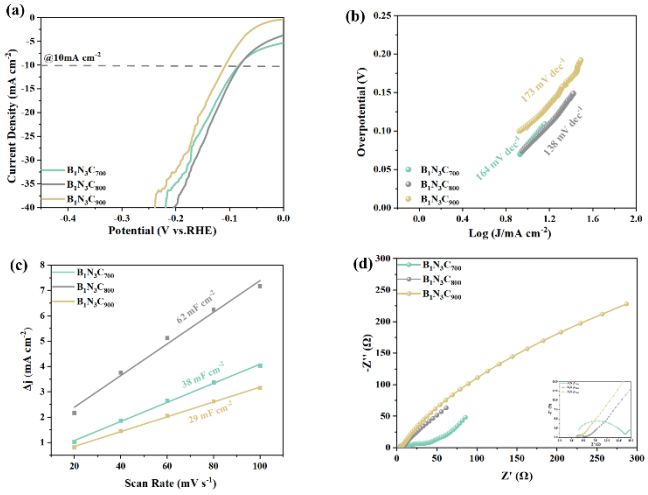

Fig S7. (a) LSV curves of $B_1N_3C_{700}$, $B_1N_3C_{800}$, and $B_1N_3C_{900}$. (b) corresponding Tafel plots. (c) C_{dl} calculated of corresponding catalysts. (d) Nyquist plots of in $B_1N_3C_{700}$, $B_1N_3C_{800}$, and $B_1N_3C_{900}$ in 0.5 M H_2SO_4 electrolyte.

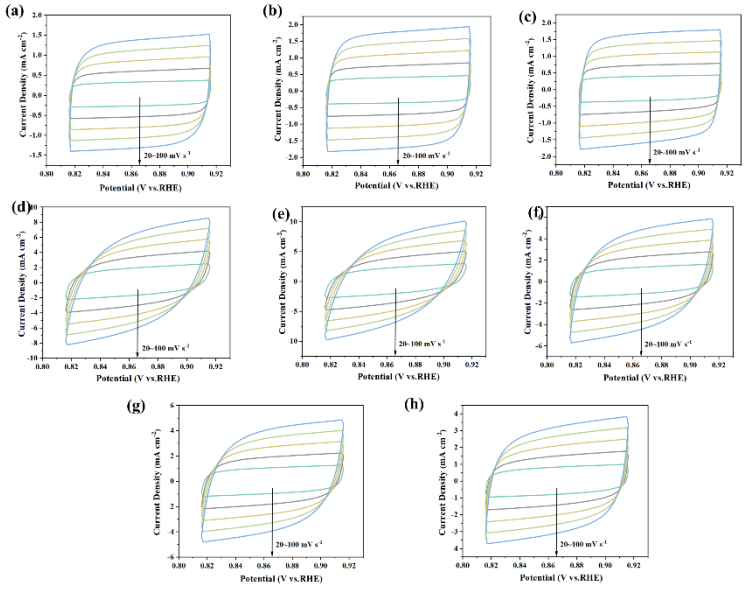

Fig. S8 Cyclic voltammograms of different electrodes in 0.5 M H_2SO_4. (a) The C_{800} electrode. (b) The B_1C_{800} electrode. (c) The N_3C_{800} electrode. (d) The $B_1N_2C_{800}$ electrode. (e) The $B_1N_3C_{800}$ electrode. (f) The $B_1N_4C_{800}$ electrode. (g) The $B_1N_3C_{700}$ electrode. (h) The $B_1N_3C_{900}$ electrode.

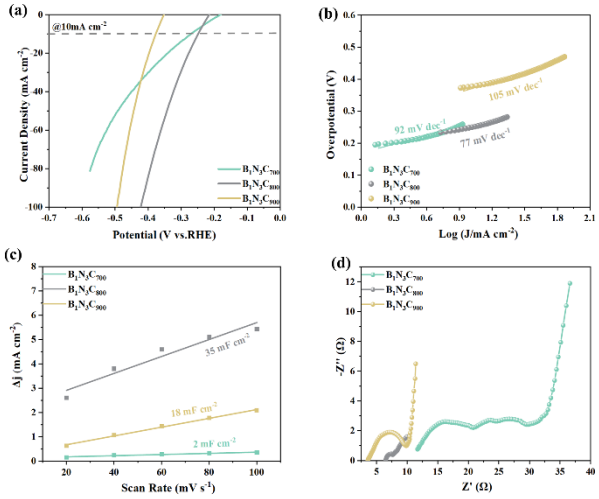

Fig. S9 Electrocatalytic HER performance of $B_1N_3C_{700}$, $B_1N_3C_{800}$, and $B_1N_3C_{900}$ in 1 M KOH. (a) LSV curves. (b) the corresponding Tafel plots of $B_1N_3C_{700}$, $B_1N_3C_{800}$,

and $B_1N_3C_{900}$. (c) C_{dl} calculated of corresponding catalysts. (d) EIS Nyquist plots of $B_1N_3C_{700}$, $B_1N_3C_{800}$, and $B_1N_3C_{900}$.

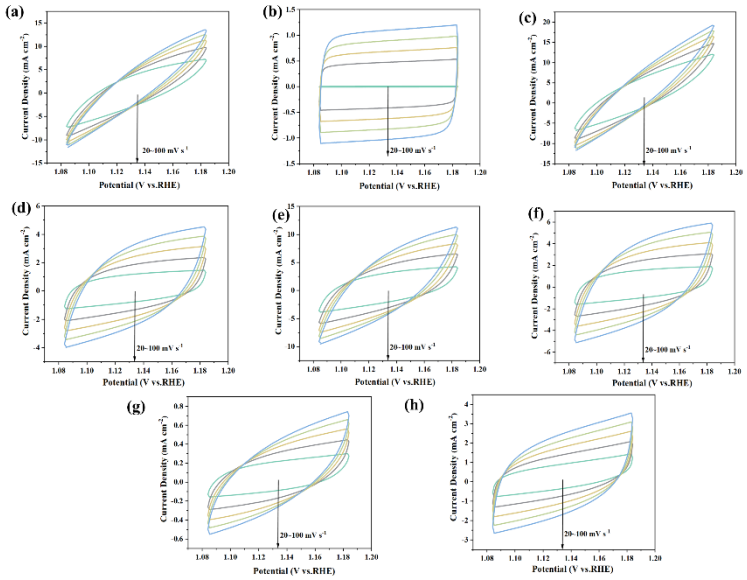

Fig. S10 The CV curves of (a) C_{800} electrodes, (b) B_1C_{800} electrode, (c) N_3C_{800} electrode, (d) $B_1N_2C_{800}$ electrode, (e) $B_1N_3C_{800}$ electrode, (f) $B_1N_4C_{800}$ electrode, (g) $B_1N_3C_{700}$ electrode, and (h)$B_1N_3C_{900}$ electrode electrodes at the scanning rate of 20 mV $s^{-1}$to 100 mV s^{-1}.

To evaluate the influence of electrode architecture, we also prepared and tested the $B_1N_3C_{800}$ in a conventional powder electrode form. In Fig. S10 and Fig. S11, the HER performance (in acidic (η_{10} = 87 mV) and alkaline (η_{10} = 224 mV) media) of the $B_1N_3C_{800}$ powder electrode is comparable to, and in some metrics even slightly better than, that of the original monolithic electrode (in acidic (η_{10} = 82 mV) and alkaline (η_{10} = 249 mV) media). This confirms the material's intrinsic activity is independent of the electrode architecture. It is worth noting, however, that the powder electrode requires more intricate preparation and testing procedures, which may limit its practical deployment despite the promising activity.

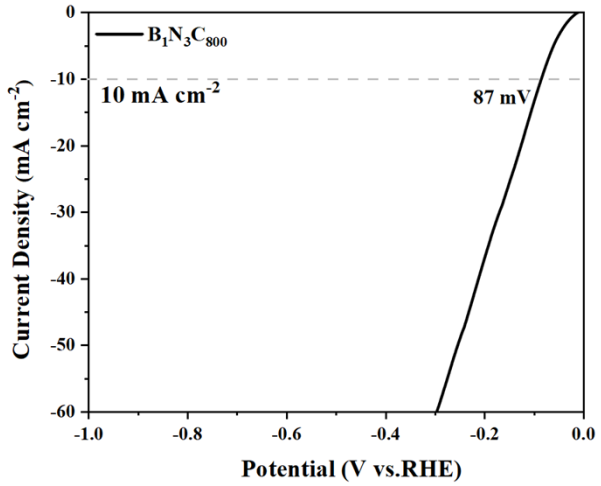

Fig. S11 HER polarization curve for the $B_1N_3C_{800}$ powder electrode in 0.5 M H_2SO_4.

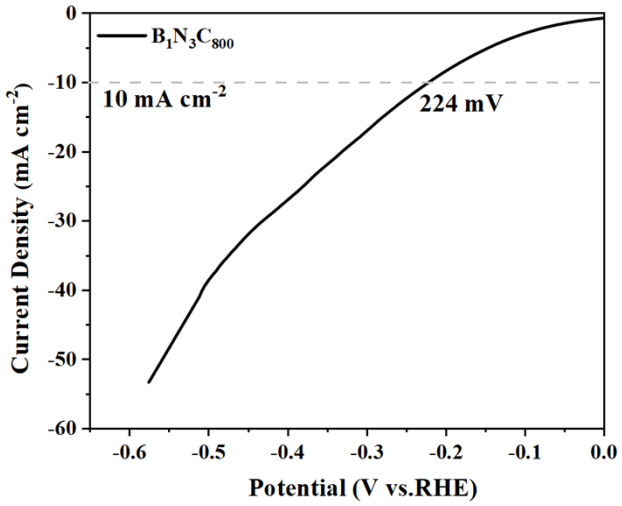

Fig. S12 HER polarization curve for the $B_1N_3C_{800}$ powder electrode in 1 M KOH.

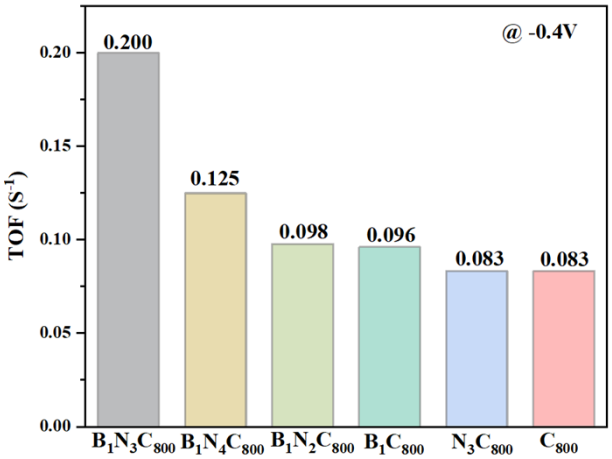

Fig. S13 The TOF value calculated at a potential of −0.4V in 1 M KOH.

Table S1 Resistance fitted according to the Nyquist plots of different samples in 0.5 M H_2SO_4.

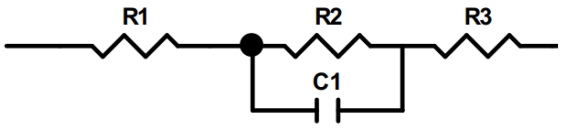

Sample	R_{sol} (Ω)	R_{ct} (Ω)	C	R_3 (Ω)
C_{800}	3.54	5.19	0.003	2430
B_1C_{800}	2.75	5.79	0.005	1154
N_3C_{800}	3.11	3.92	0.006	1202
$B_1N_3C_{700}$	3.62	7.63	0.0009	6.95
$B_1N_2C_{800}$	3.40	5.01	0.039	6.03
$B_1N_3C_{800}$	3.51	3.47	0.06	6.27
$B_1N_4C_{800}$	3.50	4.78	0.021	5.78
$B_1N_3C_{900}$	3.52	4.20	0.007	5.0

Table S2 Resistance fitted according to the Nyquist plots of different samples in 1.0 M KOH.

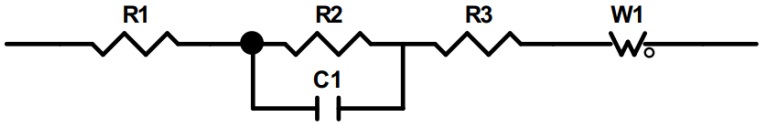

Sample	R_{sol} (Ω)	R_{ct} (Ω)	C	R_3 (Ω)	*Wo-R*	*Wo-T*	*Wo-P*
C_{800}	3.12	2.65	-	4.52	2.46	3.67	0.45
B_1C_{800}	3.26	1,87	-	4.54	2.32	4.34	0.41
N_3C_{800}	3.99	1.91	-	5.52	2.76	4.14	0.44
$B_1N_3C_{700}$	9.74	13.29	0.01	10.13	-	-	-
$B_1N_2C_{800}$	4.01	2.63	-	5.23	8.12	17.95	0.43
$B_1N_3C_{800}$	6.27	1.75	0.004	2.77	-	-	-

$B_1N_4C_{800}$	5.11	2.78	-	7.62	5.59	12.01	0.45
$B_1N_3C_{900}$	3.27	6.53	-	8.77	4.76	11.2	0.45